Computational Fluid Dynamics Analysis of Surgical Approaches to Bilateral Vocal Fold Immobility

Gabriel Rios; Robert J. Morrison, MD ⓘ; Yi Song; Shanik J. Fernando, MD; Christopher Wootten, MD;
Alexander Gelbard, MD ⓘ; Haoxiang Luo, PhD

Objectives: Bilateral vocal fold immobility (BVFI) is a rare and life-threatening condition in which both vocal folds are fixed, resulting in airway obstruction associated with life-threatening respiratory compromise. Treatment of BVFI is largely surgical and remains an unsatisfactory compromise between voice, breathing, and swallowing. No comparisons between currently employed techniques currently exist. We sought to employ computational fluid dynamics (CFD) modeling to delineate the optimal surgical approach for BVFI.

Methods: Utilizing clinical computed tomography of BVFI subjects, coupled with image analytics employing CFD models and subject pulmonary function data, we compared the airflow features in the baseline pathologic states and changes seen between endoscopic cordotomy, endoscopic suture lateralization, and posterior cricoid expansion.

Results: CFD modeling demonstrated that the greatest airflow velocity occurs through the posterior glottis on inspiration and anterior glottis on expiration in both the normal condition and in BVFI. Glottic airflow velocity and resistance were significantly higher in the BVFI condition compared to normal. Geometric indices (cross-sectional area of airway) were lower in posterior cricoid expansion surgery when compared to alternate surgical approaches. CFD measures (airflow velocity and resistance) improved with all surgical approaches but were superior with posterior cricoid expansion.

Conclusion: CFD modeling can provide discrete, quantitative assessment of the airflow through the laryngeal inlet, and offers insights into the pathophysiology and changes that occur after surgery for BVFI.

Key Words: Bilateral vocal fold immobility, posterior glottic stenosis, computational fluid dynamics, CAD/CAM, three-dimensional modeling.

Level of Evidence: NA

Laryngoscope, 130:E57–E64, 2020

INTRODUCTION

Bilateral vocal fold immobility (BVFI) is a rare condition resulting from fixation or paralysis of the true vocal folds. Etiologies of BVFI are numerous but broadly result from fibrotic restriction of cricoarytenoid joint mobility or neurogenic injury with resultant recurrent laryngeal nerve paralysis.[1,2] Injury leads to loss of dynamic glottic movement, resulting in airway obstruction.

The most effective surgical treatment for BVFI is tracheostomy, for which the level of obstruction is bypassed by placement of an airway prosthesis into the trachea.[1] The remaining surgical treatments for BVFI are primarily destructive in nature and often unsatisfactory, with the primary goal of increasing the caliber of the glottic aperture to alleviate dyspnea while keeping the vocal folds sufficiently approximated to allow production of voice and mitigate aspiration. The most commonly employed surgical techniques include posterior cordotomy, often in conjunction with partial or total arytenoidectomy, suture lateralization, and posterior cricoid split with grafting. Posterior cordotomy involves an endoscopic incision made through one of the vocal folds using a laser, allowing the incised vocal fold to shorten and displace anteriorly.[3] Suture lateralization, a potentially reversible intervention, can be employed in circumstances of neurogenic injury in which the cricoarytenoid complex remains mobile and involves endoscopic lasso of the vocal fold with a permanent suture that is secured into the soft tissues of the neck, pulling the vocal fold away from midline.[4,5] Posterior cricoid expansion with cartilage grafting serves to expand the distance between the cricoarytenoid joints, thus creating a triangular glottic inlet, and may be employed via either an endoscopic or open technique.[6,7]

Two of the primary challenges in treatment of BVFI are quantifying the degree of respiratory limitation and counseling the patient on expected functional change after surgical intervention. Pulmonary function testing (PFTs) has been found to be a useful tool in the diagnosis and surgical decision making of laryngotracheal stenosis.[8] Investigators have employed PFTs to quantify improvement in

respiratory capacity after cordotomy and glottic expansion procedures in BVFI.[9,10] Computational fluid dynamics (CFD) is a field of applied mathematics in which the movement of gaseous fluids (such as air) through a three-dimensional (3D) geometric structure is mathematically simulated, providing insight and quantitative analysis of resistance, turbulence, and particle deposition.[11] Researchers have begun to employ CFD together with geometries obtained from computed tomography (CT) and magnetic resonance imaging to assess airflow characteristics of the large airways.[11,12] These techniques have also been adapted to patients with subglottic and tracheal stenosis.[13–15]

CFD has been found to be useful by some investigators in the surgical planning and postoperative assessment of patients with subglottic and tracheal stenosis.[16,17] Markow et al. have utilized CFD to assess the change in airflow for a pediatric patient who underwent cricotracheal resection for subglottic stenosis.[18] However, there is currently a lack of understanding of the differences in physiologic impact of the various surgeries offered for BVFI. As such, a need exists to quantify the impact of the different surgical interventions employed for BVFI on glottic airflow in order to better understand potential functional improvements and guide patients toward the best procedure.

BVFI is a rare condition, which limits the ability of clinicians and investigators to study and understand the disease process or quantify the benefit of different treatments. One approach to the study of rare diseases is to pool experiences of multiple centers, which is often time, cost, and labor prohibitive. In the absence of the ability to increase the number of subjects studied, a better understanding of rare diseases can often be provided by developing new tools to quantify a specific aspect of the disease process. In this study, we employed CFD modeling as a tool to better understand the flow characteristics of glottic level airway obstruction and define the changes in glottic airflow seen with the most commonly employed surgical procedures of BVFI.

MATERIALS AND METHODS

Subject Information

Noncontrasted CT imaging of three healthy female subjects and three female BVFI subjects with comparable demographics and anthropromorphics were used for this study. CT studies were obtained prior to any surgical intervention for BVFI. The healthy subjects were used to generate normative data.

Subject Imaging, Segmentation, and Model Construction

Imaging of all study subjects was performed using noncontrasted multidetector CT with fine cuts through the larynx (slice thickness = 1.0 mm). For subjects with BVFI, imaging was obtained as part of standard preoperative evaluation for laryngotracheal stenosis. For normal subjects, CT imaging was obtained for other indications with the true vocal folds in the quiescent position. Digital Image Communication in Medicine images of each subject exam were imported into the open-source SimVascular (version 2017.08.22, http://simvascular.github.io/) medical segmentation and computer-aided design software. A 3D model of the airspace of the pharynx, larynx, and trachea was then generated via spline-based segmentation using the outline function to create contour plots of the luminal air–soft tissue interface (Fig. 1A). The model was segmented to specifically define the airspace because this was the area of interest for study of airflow dynamics. Contours plots were repeated along the axial direction for each subject, with each 3D
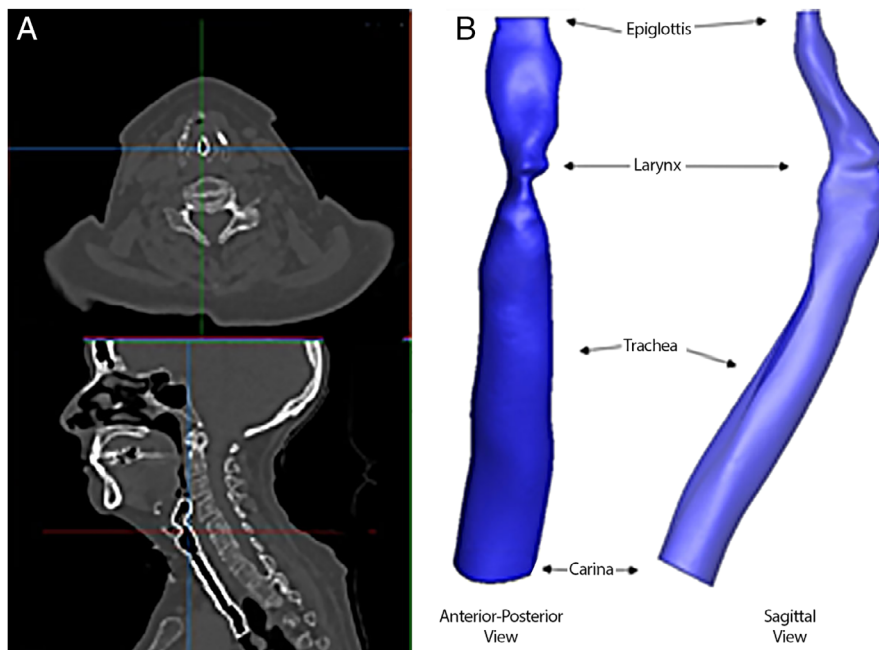

Fig. 1. Spline-based segmentation of the upper airway using SimVascular (version 2017.08.22, http://simvascular.github.io/). (A) Representative images of spline contouring of the airspace in computed tomography study of one of the three subjects with bilateral vocal fold immobility. (B) Representative generated three-dimensional airway model of one of the three subjects with bilateral vocal fold immobility.

model generated from 35 to 45 contours that defined the geometry of the larynx and trachea (Fig. 1B). If the subject had a preexisting tracheostomy, this portion of the segmentation was contoured, assuming the tracheostomy tube was removed and the tracheostoma was closed to eliminate any concurrent tracheal stenosis or tracheocutaneous fistula in the model. Two BVFI subjects had tracheostomies at the time of imaging. Segmentation was truncated cephalad at the axial level of the epiglottis and caudally at the axial level of the carina to reduce complexity of the airspace and computational expense.

Simulating Surgical Cuts

Each pathological subject studied involved creation and analysis of four model states. The first model state was the baseline pathologic state, which was segmented from CT imagery without modification. The second, third, and fourth models simulated possible surgeries on the glottis, including cordotomy, suture lateralization, and posterior cricoid expansion. For each simulated surgery, the axial contours of the air–soft tissue interface at the level of the glottis were hand-modified by a senior laryngologist (A.G.) by manipulating the control points of the contour plots. The virtual surgical procedure was applied on multiple axial planes at the level of the glottis to simulate the surgery. The number of contours modified varied per subject dependent on their anatomy but encompassed the glottis through the conus elasticus. The 3D surface was then generated through interpolation from the segmentation contours in SimVascular to create a smooth shape of the modified glottic geometry. Pre- and postoperative images from the practice of the senior author (A.G.) were utilized to estimate the expected changes of the
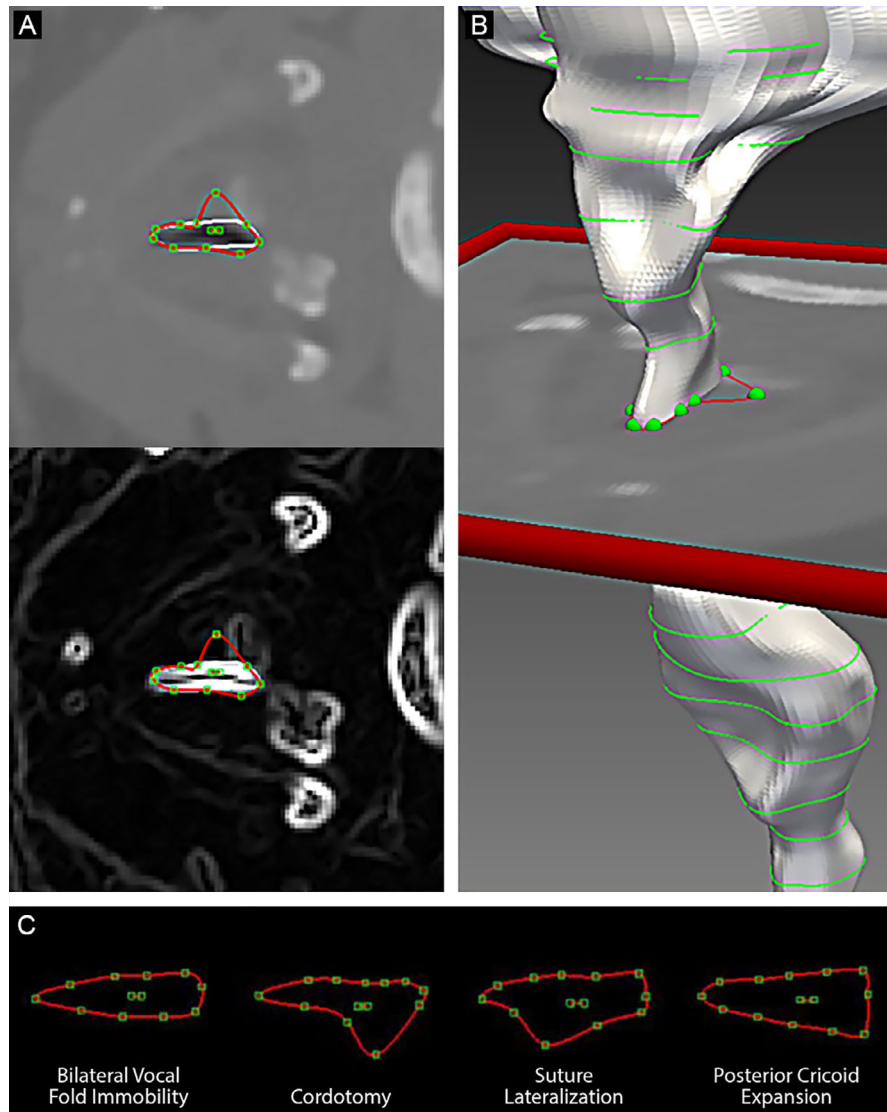

Fig. 2. Simulation of glottic procedures for bilateral vocal fold immobility in SimVascular (version 2017.08.22, http://simvascular.github.io/). (A) Example of glottic segmentation spline with control points modified to simulate cordotomy with reduction of tissue anterior to vocal process. Modifications were applied on multiple axial planes at the level of the glottis, and the three-dimensional surface was generated through interpolation from the segmentation contours to create a smooth shape of the modified geometry to simulate the expected surgical change. (B) Glottis shown in relationship to remainder of airway model. (C) Representative segmentation splines of the glottis of one of the bilateral vocal fold immobility subjects after virtual cordotomy, suture lateralization, and posterior cricoid expansion is performed in SimVascular.

glottis for each of the simulated surgical states. For example, in unilateral cordotomy, the segmentation contour of the glottis is pulled lateral in front of the vocal process in a keyhole configuration unilaterally, in keeping with the lateral incision and reduction of tissue typically performed with cordotomy (Fig. 2A). Following modification of the segmentation contours, the 3D models of the larynx and trachea are regenerated in SimVascular and then exported into COSMOL Multiphysics (version 5.2a; COMSOL Group, Stockholm, Sweden) via the methods summarized below, generating the four potential model states. Fig. 2C shows representative changes of the segmentation contours at the glottic level of one of the BVFI subjects.

CFD Model Setup

The 3D models were then exported from SimVascular as. IGES files and imported into COMSOL Multiphysics (COMSOL Group) for volumetric meshing and subsequent flow simulation. The airflow was assumed to be incompressible due to its' low Mach number (Mach 0.3). Only the steady state was considered rather than the transient simulation of a respiratory cycle. This is because a normal respiratory cycle is relatively slow as compared with the fluid dynamics inside the airway. Thus, a constant velocity normal to the inlet surface was specified. This velocity was set to be 0.889 meters per second (m/s) for inspiration and 0.806 m/s for expiration. These variables were generated via analysis of PFT data obtained from the three normal subjects. We specified this velocity at the carina to minimize the effect the uniform flow assumption would have on the flow pattern in the glottis because this was the end of the model farthest away from the glottis. The gage pressure at the epiglottis was set to zero pascals. Air density and viscosity at 20°C and the standard atmospheric pressure were assumed.

The flow field for each airway model was simulated using the Reynolds averaged Navier-Stokes (RANS) solver, as a moderate turbulence is expected in the present flow (2,000 < Re < 15,000). The SST k-ω model, one of the most commonly used turbulence models, was employed in the RANS solver to handle the turbulence behavior. During meshing, the volume of the airway was discretized into a mesh with the near lumen region refined using thin elements to resolve the boundary layer of the airflow. The laryngeal volume mesh consisted of primarily tetrahedral elements, with each model containing 0.8 to 1.4 million elements in total. To ensure the mesh resolution was sufficient, one subject model was further refined by doubling the number of mesh elements. Comparison simulations were run between the baseline and refined meshes, with an error of

TABLE I.
Cross-sectional Area and Airflow Characteristics at the Glottis Pre- and Postsimulated Surgical Cuts in Bilateral Vocal Fold Immobility Models.

		Area (cm^2)	Δ%	V_{max} (m/s)	Δ%	Δ Pressure (Pa)	Δ%
BVFI 1	BASE	0.174	–	10.48	–	82.49	–
	CDT	0.207	18.97	7.91	−24.52	47.69	−42.19
	SL	0.236	35.63	6.70	−36.07	40.74	−50.61
	PCE	0.260	49.43	6.32	−39.69	38.10	−53.81
BVFI 2	BASE	0.504	–	9.64	–	54.20	–
	CDT	0.558	10.71	7.74	−19.71	42.68	−21.25
	SL	0.601	19.25	8.29	−14.00	44.69	−17.55
	PCE	0.843	67.26	5.92	−38.59	27.95	−48.43
BVFI 3	BASE	0.229	–	9.78	–	52.36	–
	CDT	0.296	29.26	7.13	−27.10	31.85	−39.17
	SL	0.338	47.60	6.97	−28.73	30.95	−40.89
	PCE	0.449	96.07	4.63	−52.66	19.46	−62.83

BASE = baseline model without intervention; BVFI = bilateral vocal fold immobility model; CDT = cordotomy model; PCE = posterior cricoid expansion model; SL = suture lateralization model.

<7.7% for resistance and <2.1% velocity results. Thus, the baseline mesh was deemed sufficient in resolving the flow.

RESULTS

CFD models for all three normal subjects and all four possible states of the pathologic subjects (baseline, post-cordotomy, postsuture lateralization, and postposterior cricoid expansion) were generated. For the normal subjects, the maximum inspiratory airflow velocity at the glottic aperture is less than 4.5 m/s. There was a corresponding increase in airflow velocity related to decreasing glottic cross-sectional area seen in the BVFI subjects, with airflow velocities reaching as high as 12 m/s. Heat maps of airflow velocity at the glottis indicate a general shift in the flow pattern within the glottis during respiration, with airflow more posterior during inspiration and more anterior during expiration (Fig. 3). The extent of these trends varies among the subjects
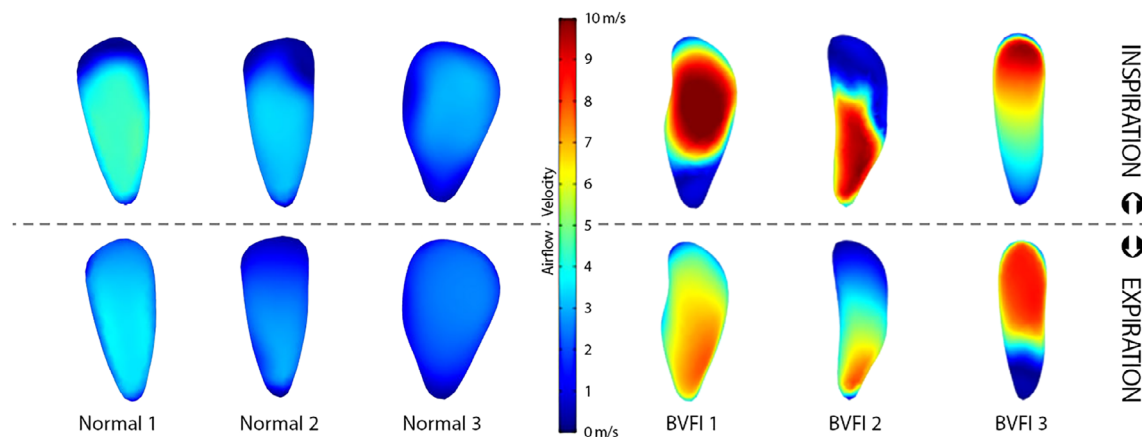

Fig. 3. Color map of airflow velocity at the level of the glottic aperture in the normal (left) and pathologic (right) conditions during inspiration and expiration. BVFI = bilateral vocal fold immobility model.

because this shift has to do, in part, with the overall curvature of the airway in the sagittal plane, which varies significantly across the subjects used in this study.

Analysis of cross-sectional area and airflow velocity at the glottic aperture in the pre- and postsurgical states of the three BVFI subjects demonstrates that overall there is a reduction in peak airflow velocity during inspiration after cordotomy, suture lateralization, and posterior cricoid expansion, with a corresponding increase in glottic cross-sectional area. There was variability in the absolute cross-sectional area, airflow velocity, and transglottic pressure change (ΔP) between the three subjects (Table I), which is consistent with the heterogeneity of this disease. The average relative decrease in maximal airflow velocity during inspiration was $25.7 \pm 3.8\%$ in cordotomy, $26.3 \pm 11.2\%$ in suture lateralization, and $42.6 \pm 8.7\%$ in posterior cricoid expansion (Table I). Posterior cricoid expansion provided the greatest benefits in glottic cross-sectional area (49%, 67%, and 96% improvement, respectively) with corresponding superior performance in airway velocity and pressure gradient changes. Comparing suture lateralization and cordotomy, suture lateralization typically had a relative greater improvement in cross-sectional area, but this did not correlate to better airflow velocity or resistance than cordotomy. Color maps of airflow velocity at the glottis demonstrate that the three surgical interventions had different impacts on the flow pattern at the glottis (Fig. 4, left). From the
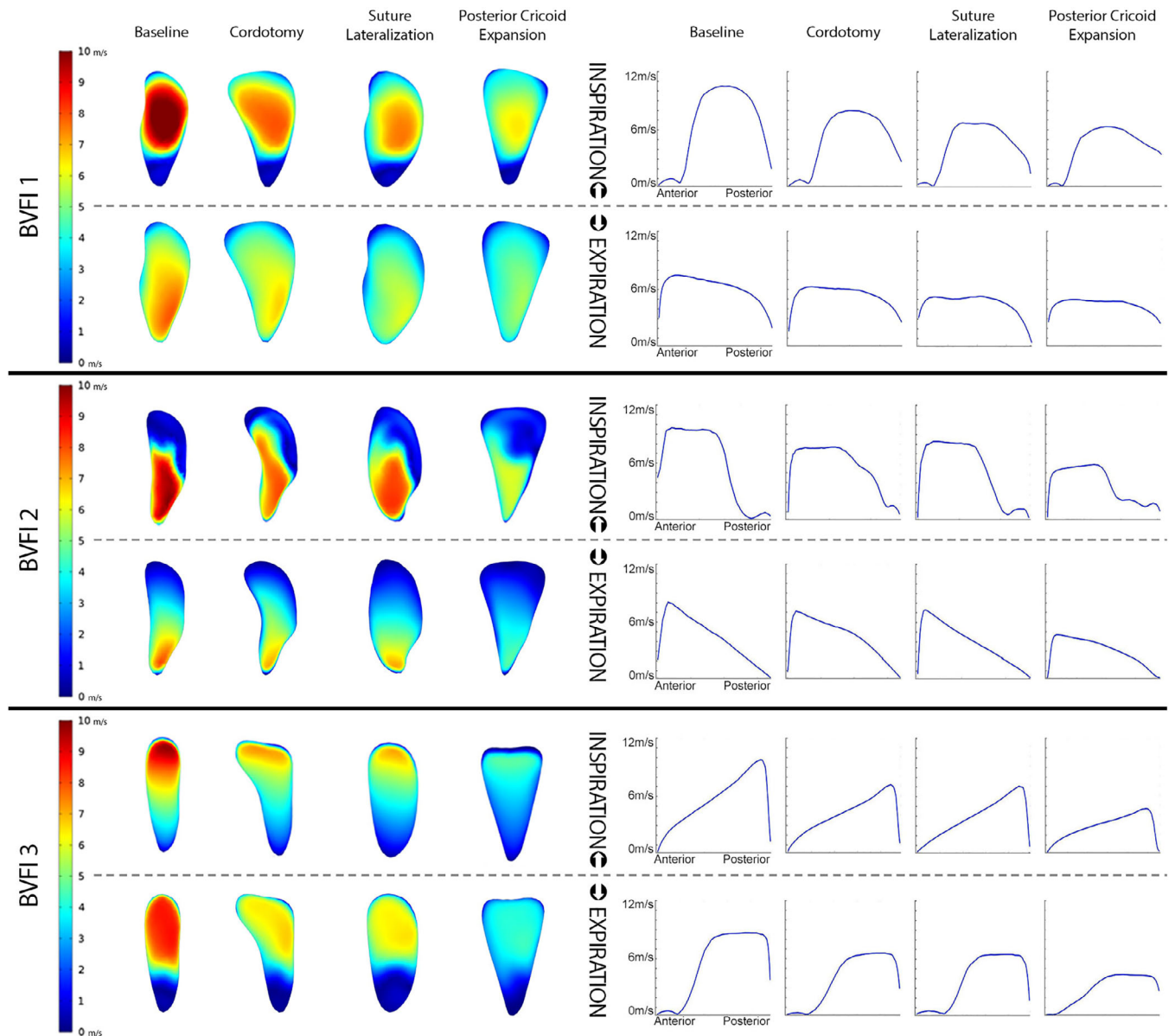

Fig. 4. Airflow velocity results of postsurgical states for BVFI. (Left) Color map of airflow velocity at the level of the glottic aperture during inspiration (above dotted line) and expiration (below dotted line) after computer simulation of cordotomy, suture lateralization, and posterior cricoid expansion. (Right) Airflow velocity at the glottic aperture plotted along the anteroposterior axis. BVFI = bilateral vocal fold immobility model.
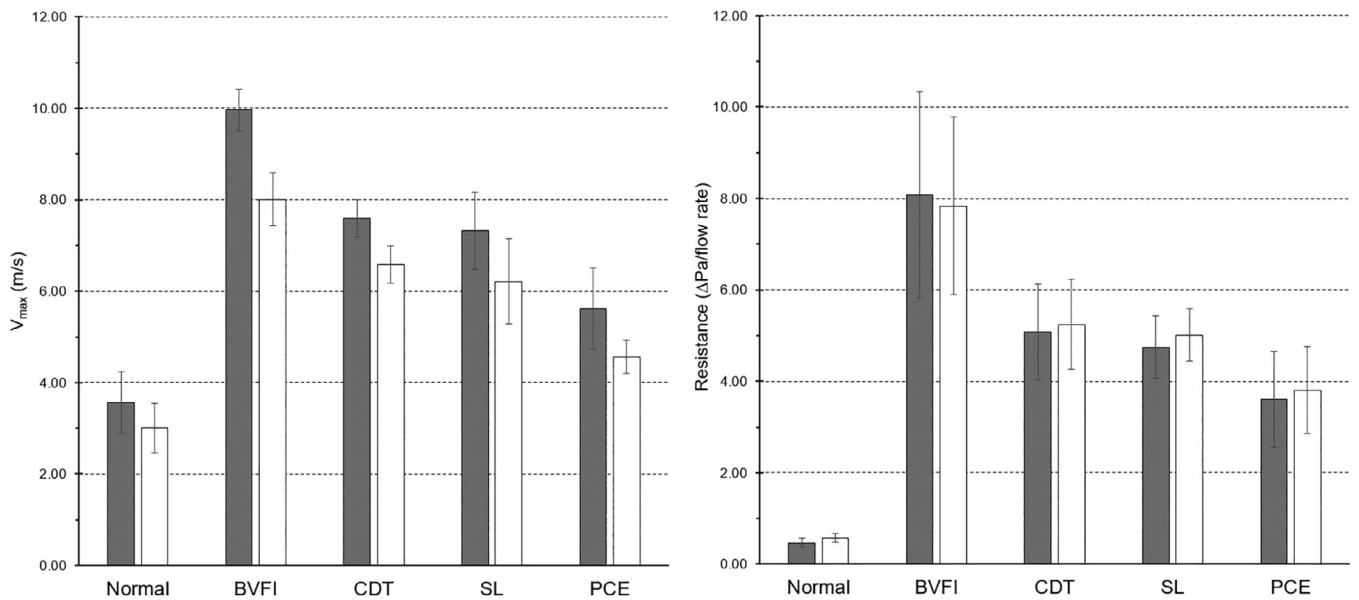
Fig. 5. Plot of average airflow velocity and airway resistance (ΔPa/flow rate) through the glottis for all simulated conditions. Results are averaged over the three subjects. Gray bars are inspiration and white bars are expiration. Resistance: Change in transglottic pressure divided by airflow rate in liters/second. ΔPa: Change in transglottic pressure in mm Hg.BVFI = bilateral vocal fold immobility models without intervention; CDT = cordotomy; PCE = posterior cricoid expansions; SL = suture lateralization.

streamline plot for a sagittal slice (Supporting Fig. S1), we can see that the flow is significantly smoother near the glottis for the surgical models as compared with the pathological models, in which large flow recirculation due to the presence of BVFI can be observed.

Airflow velocity was plotted along the anteroposterior axis of the glottis in BVFI models to better characterize the changes in airflow seen with each surgical state. This demonstrates that a similar airflow configuration is maintained in the baseline and postsurgical states, with maximal airflow seen in the posterior glottis during inspiration (Fig. 4, right). In general, there was broadening of airflow velocities in the anteroposterior axis with posterior cricoid expansion compared to the other surgical states, which would indicate redistribution of airflow out of the posterior glottis. This phenomenon was seen with both inspiration and expiration. Figure 5 demonstrates that although all three surgical interventions can reduce the maximum flow speed through glottis as well as the flow resistance, their flow speed and resistance are still much higher compared with those in the normal state. Posterior cricoid expansion produced favorable flow velocity and resistance as compared with cordotomy and suture lateralization. In Figure 5, the velocity through the glottis is higher for inspiration because we specified a higher velocity at boundary for inspiration (0.889 m/s) than for expiration (0.806 m/s). Thus, the flow rate Q is higher for inspiration. Although greater flow rate generally leads to greater pressure drop (ΔP), in the calculation the air resistance is defined as ΔP/Q. Therefore, greater resistance for the expiration indicates that the asymmetry between the inlet (supraglottis) and outlet (carina) in the airway leads to directional dependence of the resistance for the flow.

DISCUSSION

Treatment of glottic level airway obstruction secondary to BVFI is largely a surgical endeavor and remains an unsatisfactory compromise between voice, breathing, and swallowing. Like many rare conditions, there is a lack of understanding of the physiologic changes seen with BVFI, how this correlates to the patient experience of living with the condition, and the various surgical interventions for BVFI. This study represents the first to the authors' knowledge attempting to better understand the characteristics of glottic airflow in BVFI and the airflow resistance changes seen with cordotomy, suture lateralization, and posterior cricoid expansion. We also demonstrate that patient PFT data can be integrated into CFD modeling.

The results from our model confirm a long-standing belief that the majority of inspiratory airflow occurs through the posterior glottis, whereas the majority of expiratory airflow occurs through the anterior glottis. Gokcan et al. have previously described how the configuration of the glottis is important for airflow resistance in BVFI.[19] Because BVFI primarily produces airflow resistance on inspiration, our results are concordant with the surgical principle that posterior glottic intervention is the best approach to mitigate dyspnea with BVFI. It also provides a possible explanation of why nasal breathing, where the inspiratory airflow is humidified and directed in a more posterior vector, is subjectively easier for patients with BVFI. However, this is merely an inference without incorporation of the nasal cavity and oral cavity into the CFD simulation.

Our results show that all surgeries have beneficial results on airflow velocity and resistance at the level of the glottis. Posterior cricoid expansion demonstrated a larger increase in glottic cross-sectional area and more favorable

airflow velocity and resistance. The authors have anecdotally noted that patients undergoing PCE subjectively experience the most improvement in dyspnea. This may be attributable to the fact that increased cross-sectional gains with PCE are mostly in the posterior glottis. The triangular configuration of the glottic inlet may also explain this difference because our results suggest that airflow is redistributed more broadly across the anteroposterior axis of the glottis during inspiration. Despite improvements, the airflow characteristics of all surgical models still did not approach normal levels. This seems in concordance with clinical experience, where preoperative counseling will typically encompass a discussion on trying to make things "better" but not "normal."

Markow et al. have previously demonstrated in a CFD model that for patients with BVFI who achieve a glottic cross-sectional area of greater than 40 mm^2 (after cordotomy and medial arytenoidectomy), there is no significant further reduction in airflow resistance with further cross-sectional gains.[18] Our second BVFI subject has cross-sectional areas greater than this in the baseline state and had favorable improvements in airflow resistance with additional glottic expansion. Markow et al. segmented the glottic configuration and inserted it into a cylinder to run their CFD model. In comparison, our CFD model included segmenetation of the entire larynx and trachea. It is likely that these discordant results are related, in part, to the differences in the flow created by introduction of supraglottic and tracheal airflow into the model. It is interesting to note that, although the gains in glottic cross-sectional area with suture lateralization were greater than cordotomy, the airflow characteristics between the two were similar and did not approach posterior cricoid expansion. This suggests that the relationship between cross-sectional area and airflow velocity and resistance is not linear and there are likely "inflection points" with progressive expansion where airflow parameters favorably increase. Further study integrating CFD results with validated patient-reported dyspnea outcomes and PFT testing will also provide additional insights on how quantitative changes in airflow velocity and resistance correlate to the patient's subjective experience of dyspnea with BVFI.

The other significant consideration in surgical intervention for BVFI is the impact on voicing. Prior investigators have had success generating a computational model of laryngeal vibration in the normal state.[20] Future integration of modeling for voicing on expiration into our CFD model will allow us to better delineate the vocal consequence of each procedure. The goal is to ultimately build toward an open-source model that allows a surgeon to predict the respiratory and voice outcomes of different surgical interventions for BVFI, guiding the surgeon and patient toward the best procedure.

This study serves as a template for how existing engineering techniques created for other purposes can be adapted to improve understanding of rare disorders where more empiric scientific approaches are limited by the rarity of the condition. Our study is limited in several ways. Firstly, the geometry of this model is static, which fails to account for issues with supraglottic dynamic collapse that can occur with BVFI. Secondly, all postsurgical states are based on virtual surgery performed by a senior laryngologist (A.G.), introducing bias as far as how the glottic contours were manipulated. Data would be best validated with use a CT imaging pre- and postsurgical intervention within the same individual. Additionally, given its complex geometry, it is difficult to assume a realistic velocity profile at the carina. However, we believe the carina is sufficiently located away from the glottis (the region of interest in the present study) to minimize the effect of any error in the carina boundary velocity profile by physical mixing of the flow in the trachea below the glottis. Finally, segmentation and meshing of the larynx is limited, in part, by the resolution of the CT imaging and clarity of the air–soft tissue interface. Although this was mitigated by utilizing thin-cut CT imaging, averaging for the airspace model is expected. This may have implications on computational outcomes within the glottis, where submillimeter changes in cross-sectional area can potentially change airflow characteristics. This error can be mitigated in the future by increasing the number of subjects studied via integration of CFD tools into ongoing clinical trials with international collaborative of airway investigators of the North American Airway Collaborative (NoAAC), providing further validation of the model.

CONCLUSION

CFD can be used to simulate glottic level airflow in patients with bilateral vocal fold immobility. This provides insight into the disease process and how surgical approaches can be adapted to address areas of greatest airflow resistance. Surgical simulation of cordotomy, suture lateralization, and posterior cricoid expansion all yield improvements in airflow resistance and airflow velocity in the postoperative state. Further study is required to validate the CFD model against clinical data and adapt the model to assess impact on voicing and predict postoperative improvements.

BIBLIOGRAPHY

1. Hillel AD, Benninger M, Blitzer A, et al. Evaluation and management of bilateral vocal cord immobility. *Otolaryngol Head Neck Surg* 1999;121:760–765.
2. Benninger MS, Gillen JB, Altman JS. Changing etiology of vocal fold immobility. *Laryngoscope* 1998;108:1346–1350.

3. Dennis DP, Kashima H. Carbon dioxide laser posterior cordectomy for treatment of bilateral vocal cord paralysis. *Ann Otol Rhinol Laryngol* 1989;98: 930–934.

4. Kirchner FR. Endoscopic lateralization of the vocal cord in abductor paralysis of the larynx. *Laryngoscope* 1979;89:1779–1783.

5. Lichtenberger G. Reversible lateralization of the paralyzed vocal cord without tracheostomy. *Ann Otol Rhinol Laryngol* 2002;111:21–26.

6. Lano CF, Duncavage JA, Reinisch L, Ossoff RH, Courey MS, Netterville JL. Laryngotracheal reconstruction in the adult: a ten year experience. *Ann Otol Rhinol Laryngol* 1998;107:92–97.

7. Dahl JP, Purcell PL, Parikh SR, Inglis AF. Endoscopic posterior cricoid split with costal cartilage graft: a fifteen-year experience. *Laryngoscope* 2017; 127:252–257.

8. Nouraei SA, Nouraei SM, Patel A, et al. Diagnosis of laryngotracheal stenosis from routine pulmonary physiology using the expiratory disproportion index. *Laryngoscope* 2013;123:3099–3104.

9. Nawka T, Sittel C, Arens C, et al. Voice and respiratory outcomes after permanent transoral surgery of bilateral vocal fold paralysis. *Laryngoscope* 2015;125:2749–2755.

10. Asik MB, Karasimav O, Birkent H, Merati AL, Gerek M, Yildiz Y. Impact of unilateral carbon dioxide laser posterior transverse cordotomy on vocal and aerodynamic parameters in bilateral vocal fold paralysis. *J Laryngol Otol* 2016;130:373–379.

11. Bates AJ. Chapter 5.3: Scalar distribution at successive instants. In: Mechanics of Airflow in Human Inhalation. [Dissertation]. London, UK: Imperial College of London; 2014. p. 163.

12. Chen T, Chodara AM, Sprecher AJ, et al. A new method of reconstructing the human laryngeal architecture using micro-MRI. *J Voice* 2012;26: 555–562.

13. Zdanski C, Davis S, Hong Y, et al. Quantitative assessment of the upper airway in infants and children with subglottic stenosis. *Laryngoscope* 2016; 126:1225–1231.

14. Brouns M, Jayaraju ST, Lacor C, et al. Tracheal stenosis: a flow dynamics study. *J Appl Physiol* 2007;102:1178–1184.

15. Malve M, Perez del Palomar A, Chandra S, et al. FSI analysis of a healthy and a stenotic human trachea under impedance-based boundary conditions. *J Biomech Eng* 2011;133:021001.

16. Mylavarapu G, Mihaescu M, Fuchs L, Papatziamos G, Gutmark E. Planning human upper airway surgery using computational fluid dynamics. *J Biomech* 2013;46:1979–1986.

17. Quammen CW, Taylor RM 2nd, Krajcevski P, et al. The virtual pediatric airways workbench. *Stud Health Technol Inform* 2016;220:295–300.

18. Markow M, Janecki D, Orecka B, Misiolek M, Warmuzinski K. Computational fluid dynamics in the assessment of patients' postoperative status after glottis-widening surgery. *Adv Clin Exp Med* 2017;26:947–952.

19. Gokcan MK, Kurtulus DF, Ustuner E, et al. A computational study on the characteristics of airflow in bilateral abductor vocal fold immobility. *Laryngoscope* 2010;120:1808–1818.

20. Sadeghi H, Kniesburges S, Kaltenbacher M, Schutzenberger A, Dollinger M. Computational Models of Laryngeal Aerodynamics: Potentials and Numerical Costs. *J Voice* 2018. https://doi.org/10.1016/j.voice.2018.01.001.